PAPER • **OPEN ACCESS**

Application of a General Discrete Adjoint Method for Draft Tube Optimization

To cite this article: B Fleischli *et al* 2021 *IOP Conf. Ser.: Earth Environ. Sci.* **774** 012012

View the article online for updates and enhancements.

You may also like

- Effects of a rectifier on the hydraulic stability of the draft tube
L J Yang, J Zhang, C M Yan et al.
- Physical Properties and Evolutionary States of EA-type Eclipsing Binaries Observed by LAMOST
S.-B. Qian, J. Zhang, J.-J. He et al.
- Toward the development of a label-free multiple immunosensor based on thin film transistor microelectrode arrays
Dongchen Zhu, Grant A Cathcart, Satoshi Ihida et al.

This content was downloaded from IP address 132.207.88.186 on 12/01/2023 at 13:15

IOP Conf. Series: Earth and Environmental Science **774** (2021) 012012 doi:10.1088/1755-1315/774/1/012012

Application of a General Discrete Adjoint Method for Draft Tube Optimization

B Fleischli[1], A Del Rio[1], E Casartelli[1*], L Mangani[1], B F Mullins[2], C Devals[3] and M Melot[2]

[1] Lucerne University of Applied Sciences and Arts, Technik & Architektur, Horw, Switzerland
[2] Andritz Hydro Canada Inc., Pointe-Claire, Québec, Canada
[3] École Polytechnique de Montréal, Montréal, Québec, Canada

E-mail: *ernesto.casartelli@hslu.ch

Abstract. Automatic optimization is becoming increasingly important in turbomachinery design to improve the performance of machine components and Evolutionary Algorithms (EAs) play a very important role in this task. The main drawback of EAs is the large number of evaluations that are required to obtain an "optimal" result. Consequently, in order to keep the computational time in an affordable frame for design purposes, either the mesh size has to be limited, thus reducing the resolution of the flow phenomena, or the number of free parameters must be kept small. Adjoint optimization does not suffer from these restrictions, i.e. the optimization time is not affected by the number of parameters. The computational effort for the adjoint method scales only with the grid size and is usually in the range of two times the CFD simulation alone. In this paper, a discrete adjoint method based on a coupled pressure based RANS solver is presented and applied to draft tube optimization. The adjoint solver is general and can therefore deal with any turbulence model supported by the CFD solver as well as any boundary condition, including mixing planes and mesh interfaces needed for multi-stage simulations. Furthermore, there is no restriction on the choice of objective function. The adjoint method is first applied to a baseline draft tube geometry and then again to its EA optimized geometry where the objective function was the minimization of losses in the draft tube. To reduce the complexity for this proof of concept but still including multiple operating points in the optimization, only peak efficiency and full-load were optimized simultaneously. The adjoint optimization can significantly improve the draft tube performance in both cases (baseline and EA optimization). The interplay between local and global optimization seems to be a promising strategy to find optimal geometries for multi-operating point/multi-objective optimization and will be further investigated in subsequent research.

1. Introduction

Automatic optimization is becoming a very important tool to further optimize turbomachinery components in a more efficient way than human driven trial-and-error [1]–[6]. These methods allow the exploration of a wider design space and often lead to novel solutions. There are two main classes of optimization methods: gradient-free and gradient-based. Gradient-free methods, like evolutionary based algorithms (EAs), can be easily deployed as a "black-box" and are therefore very popular. Their main drawback is the necessarily large computational effort and time. On the other end, gradient based methods like adjoint optimization are computationally much more efficient. In this paper a general discrete adjoint method is presented and applied to the optimization of a draft tube. The draft tube plays an important role in hydroelectric power

Content from this work may be used under the terms of the Creative Commons Attribution 3.0 licence. Any further distribution of this work must maintain attribution to the author(s) and the title of the work, journal citation and DOI.
Published under licence by IOP Publishing Ltd

plants, especially when medium to high specific speed machines are involved. By converting part of the flow kinetic energy at the runner exit into pressure, an increase in efficiency of the overall system can be achieved. During the lifetime of a power plant a considerable amount of additional electrical energy can therefore be produced, which leads to an increased return on investment. In general, draft tube design is restricted by several parameters, such as stability requirements, construction costs and operating conditions.

2. Numerical set-up

The computational domain consists of an isolated model-scale draft tube without additional components of the turbine, such as the runner or spiral case (see figure 4a). The structured mesh consist of approximately 356'000 hexagonal elements and fulfills the internal quality standards of Andritz Hydro for automatic optimization purposes. Boundary layer resolution gives an averaged y^+ value in the order of 40 for the investigated operating points (OPs). Standard SST $k-\omega$ is used for turbulence modeling. It is important to note that the adjoint solver does not rely on the commonly applied frozen turbulence assumption and also integrates the turbulence equations in the adjoint problem in order to get accurate sensitivities. The temporal term is discretized as steady-state and the discretization of the flow equations is second order in space with a high resolution scheme.

The flow solver used for both optimization methods is the pressure-based block-coupled solver by Mangani et al. [7]. The governing pressure and momentum equations are implicitly coupled, producing robust simulation behavior and allowing fast convergence rates.

The velocity boundary conditions at the inlet for the two considered operating points (peak efficiency, full-load) are based on profiles obtained in previous simulations with the complete turbine model (spiral case, runner and draft tube). An averaged static pressure is set at the outlet.

3. EA optimization

3.1. Parametric design

Conventional elbow-type draft tubes are typically designed using 20 or more planar sections that are positioned along a 3-dimensional spine curve and oriented in space with respect to that curve (see figure 1). The types of shapes used to construct these sections can range from simple circles, ellipses and rectangles to more complex shapes such as ovals and radiused rectangles. After the sections are in place, a wetted surface is generated by connecting the sections using a method best-suited for the desired result. For example, ruled surfaces are used to generate "cornered" geometries that are relatively cheap and easy to fabricate with steel plates while splining techniques are used to generate "smooth" geometries that are more appropriate for concrete construction. Draft tubes are often subject to civil engineering constraints and may require the addition of one or more piers to support the weight of the roof.

A typical draft tube design of the type described above may involve upwards of 200 parameters depending on the number and types of sections used. While it is possible to optimize problems of such size, it is often impractical in a commercial turbine development context given the availability of computing resources and the time required to evaluate the performance of a single draft tube design. Therefore, it is desirable to find much simpler parametric models that are capable of generating draft tube geometries in the design space of interest, but with significantly fewer variables.

3.2. Simplified parametric model

The idea for the simplified model is to start with a fully-parameterized base design as shown in figure 1 and then deform it using several control points in order to create a new geometry. To simplify the parameterization even further, the position and orientation of the section planes

for the base design are fixed in space for all designs. The shape and size of the first two inlet sections that form the cone are also fixed, while all remaining section parameters are allowed to vary except for the shape of the outlet section, which is forced to be a rectangle so that it can connect to the extension box. A set of 4 control points are used on each side of the draft tube (left, right, roof, floor) to interpolate the actual deviations from the base design for each section (see figure 2). In our parameterization, the base draft tube design consisted of symmetric radiused rectangle sections and a pier. The shape and size of the radiused rectangle sections are controlled by width, height, floor radius and roof radius parameters. Finally, the pier is parameterized by a lateral offset parameter and a composite Bézier curve that controls the shape of the nose (see figure 2, detail A).

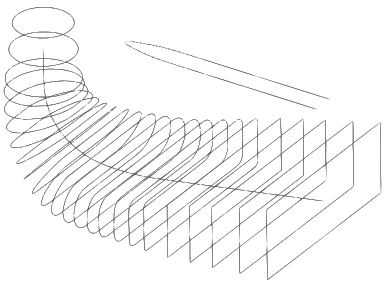

Figure 1: Conventional elbow-type draft tube.

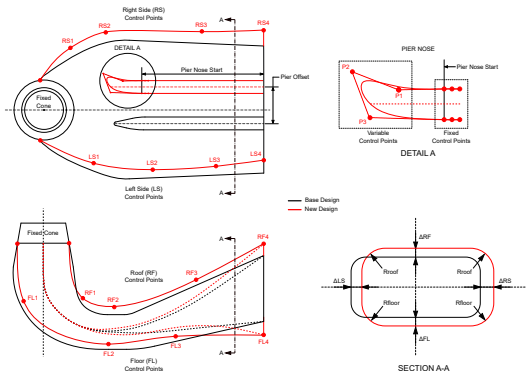

Figure 2: Simplified draft tube parametrization.

3.3. Optimization method

A metamodel-assisted evolutionary algorithm (MAEA) was used to perform the draft tube design optimization. Details on this optimization method can be found in previous work on CFD based draft tube hydraulic design optimization [1].

3.4. Optimization procedure

An Andritz Hydro in-house draft tube hydraulic design optimization tool (see [1] for details) was used to perform the optimization. The population sizes used for the MAEA were $\mu = 5$ parents and $\lambda = 40$ offspring. The performance for each draft tube was evaluated at two operating conditions—one at peak efficiency and the other at full-load—and the objective function was defined as the average of the total pressure difference between the draft tube inlet and the outlet of the draft tube extension box. In addition to the geometric constraints imposed by the simplified parametric model (see section 3.2), the area of the outlet section and the overall height of the draft tube were constrained to not exceed that of the base design. For this optimization, the simplified parametric model consisted of a base design with 24 radiused rectangle sections and a pier. A total of 47 variable parameters were used to control the creation of new draft tube geometries—40 for the generation of new sections and 7 for the pier. After the sections and

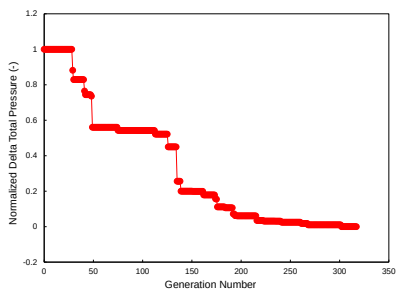

Figure 3: Optimization convergence.

pier were created and properly positioned, a splining technique was used to join the sections to create a smooth draft tube geometry for meshing and evaluation.
The optimization generated a total of 7'310 designs in 318 generations before it was terminated due to time limitations. Of the designs generated, 2'549 were actually evaluated while the remaining designs were not evaluated due primarily to invalid parameter combinations or geometry constraint failures. The total execution time converted to one core equivalent was 7'599 hours. Figure 3 shows the evolution of the objective function during the optimization.

3.5. Optimized geometry

At first glance, the final geometry of the optimized design looks quite similar to the base design except, perhaps, for the position of the pier (see figure 4). However, a closer inspection of the draft tube geometry (see figure 5) shows that there are significant differences between the base and optimized designs.

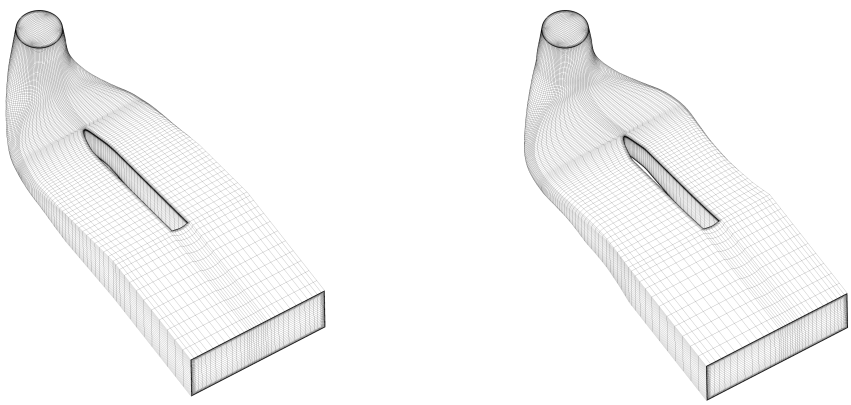

(a) Base design. (b) Optimized design.

Figure 4: Comparison of base and optimized draft tube meshes.

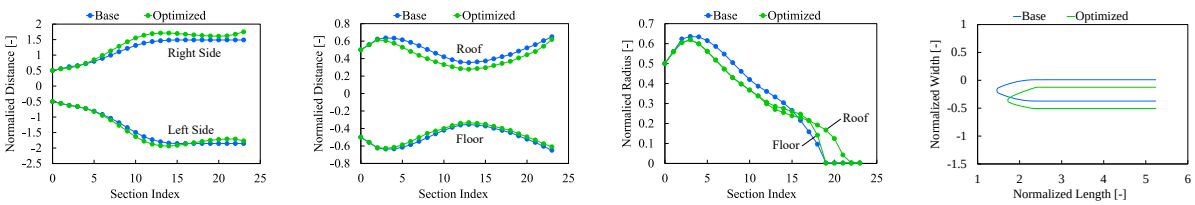

(a) Section width. (b) Section height. (c) Section radius. (d) Pier geometry.

Figure 5: Comparison of base and optimized draft tube geometries.

4. Adjoint optimization

4.1. Adjoint method

The base design and the improved geometry obtained with the previously described EA optimization were taken as starting points for the adjoint based optimization. The adjoint

method computes the gradient of the objective with respect to the mesh nodes by solving an additional linear problem—the so called adjoint problem [8]. The method can be applied for general optimizations and is not restricted by the number of parameters used. The simulations conducted in this work used a box with 10 x 10 x 10 control points as parameters, see figure 7. Furthermore, the discrete adjoint method can deal with any turbulence model supported by the CFD solver as well as any boundary condition, including mixing planes and mesh interfaces needed for multi-stage simulations. Additionally, there is no restriction on the choice of objective function. The adjoint solver used in this work is integrated in the in-house CFD coupled pressure-based flow solver of the Lucerne University of Applied Sciences (HSLU) described in Mangani et al. [7].

4.2. Optimization procedure

The entire optimization is controlled by a Python script as depicted in figure 6. The script writes the displacements of the control points Δx^c (α - file) and calls the deformation routine to produce a new mesh—initially the displacements are zero. The primal solver computes the flow solution for the given mesh. Based on the flow solution, the adjoint solver solves the adjoint equations and produces the $\frac{\partial J}{\partial x}$ - file, i.e. the sensitivity of the objective with respect to all mesh nodes. The optimization script accumulates the sensitivities on the control points (red arrows in figure 7). The displacement of the i_{th} control point x_i^c is then updated in a simple gradient descent fashion where k is a constant that defines the step size.

$$\Delta x_i^c -= k \cdot \frac{\partial J}{\partial x_i^c} \tag{1}$$

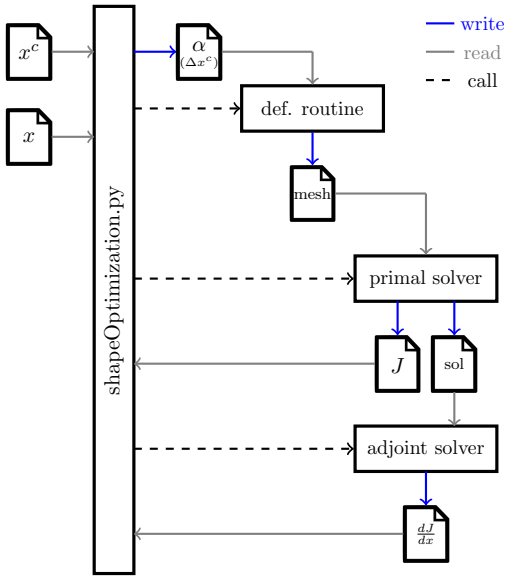

Figure 6: Adjoint shape optimization workflow.

Free-form deformation (FFD) based on Non-Uniform Rational B-Splines (NURBS) and inverse distance weighted (IDW) interpolation is used to deform surface and interior mesh nodes. With the new displacement of the control points, the loop repeats until the optimization converges at a minimum. The two operating points considered for the optimization (peak efficiency and full-load) are calculated simultaneously and the resulting gradients are superimposed with a 50/50 weighting.

The convergence behavior is shown in figures 8 and 9 for the base design and the EA optimized initial geometry (IG) at peak efficiency and full-load. The criterion J represents the rate of energy influx at the inlet. When comparing the two figures, it is noticeable that improvements can be achieved disproportionately at the full-load operating point. Nevertheless the solver is able to optimize both operating points.

Both optimizations were running with a relatively small gradient descent step size for 300 iterations. This test was conducted to evaluate the mesh deformation capability and to see how much the adjoint based method can improve the objective function in the limit. As can be seen from figures 8 and 9 the main reduction takes place in the first 50-100 iterations, which already should be sufficient for most applications. More sophisticated gradient based optimization

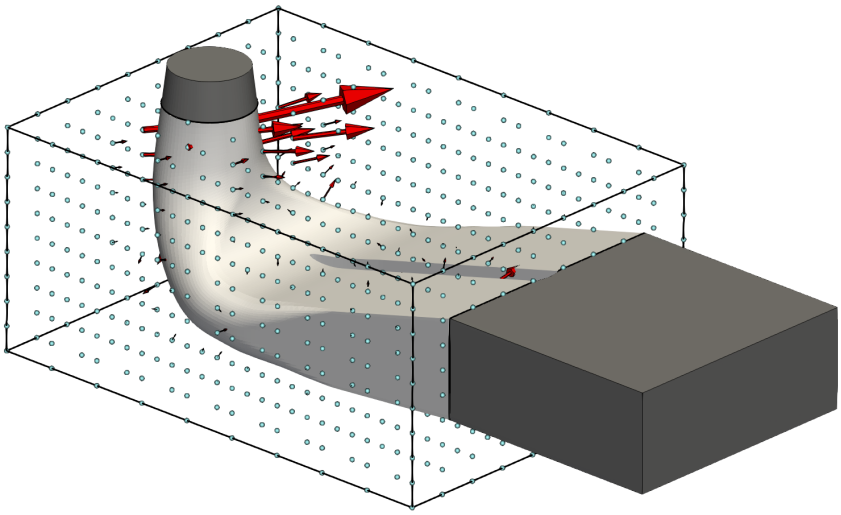

Figure 7: FFD bounding box highliting the deformable mesh region and showing the used control points with the corresponding sensitivity vectors.

techniques, eg. quasi-Newton methods, which can already be used in the implemented adjoint framework, can reduce the required number of iterations even further to the range of 20-50.
The total execution time converted to one core equivalent was 5'220 hours and 300 designs were generated and computed. Please note, that after the first 100 iterations, which took 1'740 hours and is less then a quarter of the time required for the GA optimization, already 80% of the objective function improvement is achieved. Each of these design evaluations include the flow and the adjoint solver simulation for both operating points.

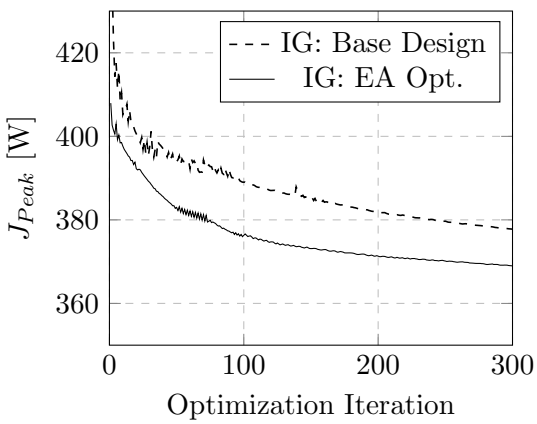

Figure 8: Adjoint convergence behavior for peak efficiency OP.

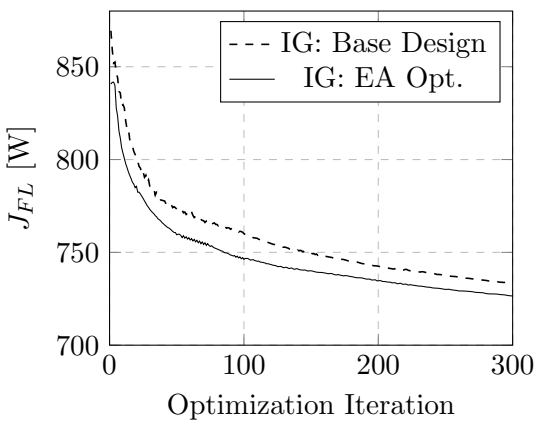

Figure 9: Adjoint convergence behavior for full-load OP.

4.3. Optimized geometry

Figure 10 compares the optimized geometry obtained with the adjoint method to the base design. The adjoint optimized geometry starting from the EA solver output shows similar patterns as in Figure 10 (b). The free-form deformation with the selected medium number of control points (1'000) produces a complex but smooth surface. The higher the control point

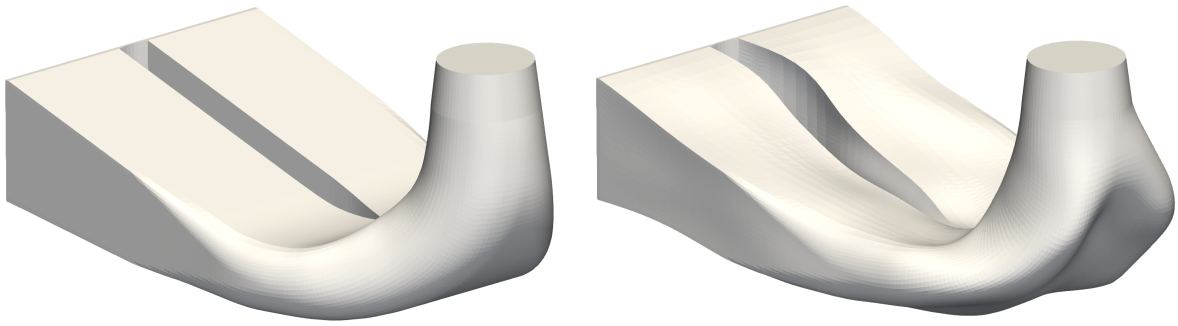

(a) Base design. (b) Adjoint optimized design.

Figure 10: Comparison of the base design (a) to the adjoint optimized geometry (b).

density for the FFD, the more features can be captured during the optimization, which leads to surfaces reminiscent of bionic structures. Practical arguments regarding manufacturing decide the degree of resolution of features and hence the complexity of the resulting geometry.

Adjoint based shape optimization with free-form deformation can also be used in a different approach. Instead of taking the optimized geometry directly for building the prototype, it is also possible to study the resulting geometry and related flow patterns, extracting important features out of it and use this knowledge in combination with a conventional parameter study to improve the classical design. In the case of the investigated draft tube one interesting feature would be the leading edge of the pier, see Figure 11. The adjoint optimization reshapes the initially straight leading edge into a form familiar from rotor blade designs. The shape varies thereby in span-wise direction. This observation can now be used for a separate 3D parameter study on the pier leading edge. The modification of the pier and in particular of the pier leading edge is a procedure often in the redesign study of draft tube geometries [9].

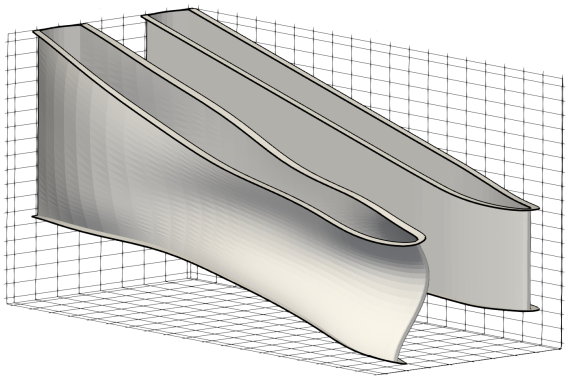

Figure 11: Adjoint optimization of the pier geometry.

5. Optimization results

5.1. Efficiency improvements

The EA optimization was able to achieve a 4.75% reduction in the average difference in total pressure between the draft tube inlet and the outlet of the extension box for both operating points. Given the lack of a definite plateau in the convergence plot (see figure 3), it is quite possible that designs with even better performance could be found if the optimization were allowed to continue.

The adjoint optimization of the base design leads to an improvement of 19.23%. Compared to the EA optimization this is an additional improvement of 14.48%. To guarantee consistency with the EA optimization, the same evaluation procedure was used. Therefore, the objective function was measured in terms of total pressure losses along the draft tube.

The result for the adjoint optimization starting from the EA shows a further improvement of 16.7%. The overall (combined) improvement with regards to the base design is therefore 21.5%.

5.2. Total pressure changes

Figure 12 (a) and (b) shows the total pressure changes along different sections of the draft tube for the base design and all optimized geometries. The total pressure is mass-flow averaged on several planes from inlet to outlet, splitting the model into its main components (inlet section (cone), elbow, pier and outlet box). A separate definition for the total pressure is used at the outlet to take into account that swirling flow and high velocity spots have to be regarded as losses. The dynamic pressure contribution in this section was therefore calculated by the reference velocity derived from the mass flow and the area of the outlet.

Losses along the draft tube are significantly higher for the full-load OP (see figure 12 (b)) compared to peak efficiency OP (see figure 12 (a)), as expected. The losses in the elbow and pier segments are significantly reduced by the adjoint optimization, whereas no major variations can be identified with the GA optimization.

The main improvements compared to the base design are achieved in the last section, the outlet box. At first sight, it may seem small improvement has been achieved because performance of turbines in laboratory tests is evaluated at the outlet of the pier. However, the reduction in total pressure loss in the outlet box, which would be the tail race of an actual turbine, would result in a reduced back-pressure, meaning that slightly lower head would be required to drive the flow through the turbine. Considering the losses from cone inlet to the end of the pier, only the adjoint solutions present an improvement compared to the base design, while the EA geometry up to this location is even slightly worse. These observations suggest that the reduction of flow non-uniformity and swirl are the main driving factors for all three optimizations.

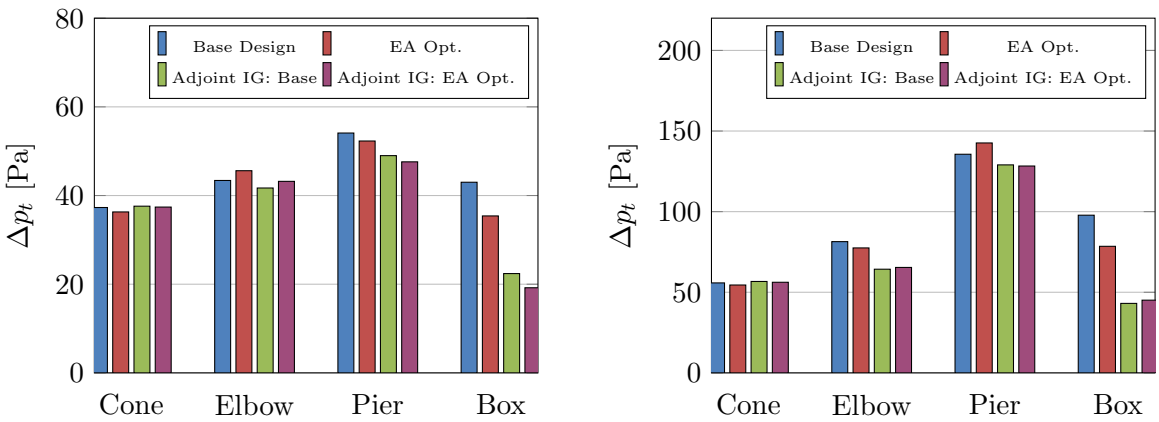

(a) Peak efficiency OP. (b) Full-load OP.

Figure 12: Change in mass-flow averaged total pressure Δp_t along the draft tube.

5.3. Local flow structures for full-load OP

Figures 13 (a-d) show 3D streamlines through the left channel of the pier (in flow direction). Backflow zones are highlited by iso-volumes of negative x-velocity colored in green.

All optimizations were capable of eliminating the backflow in the channel left of the pier. Additionally, also the recirculation zone at the pier trailing edge and the swirl component in general were substantially reduced in case of the adjoint optimizations.

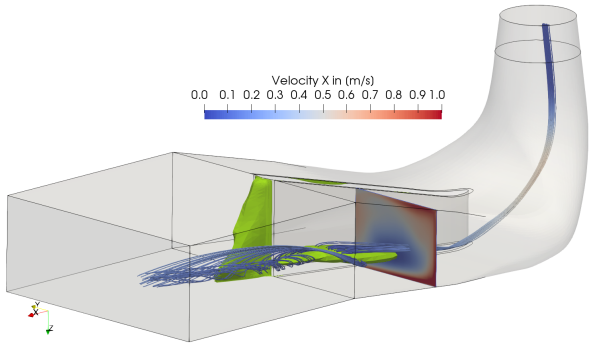

(a) Base design.

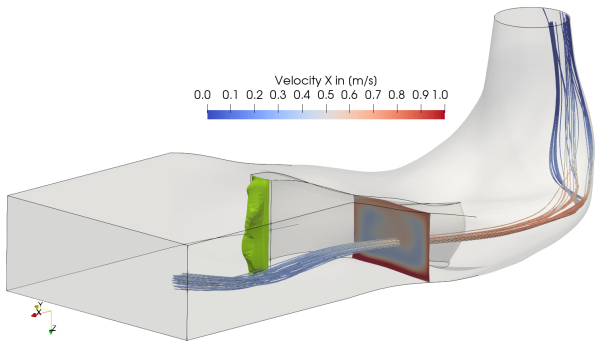

(b) Adjoint optimized design (IG: Base design).

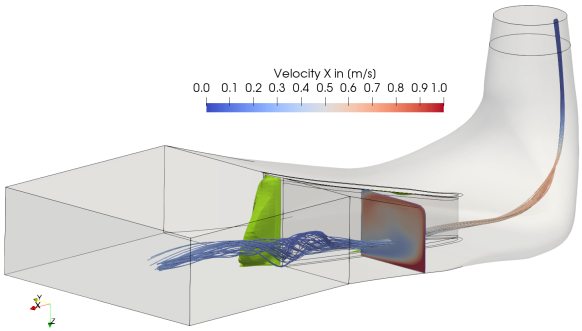

(c) EA optimized design.

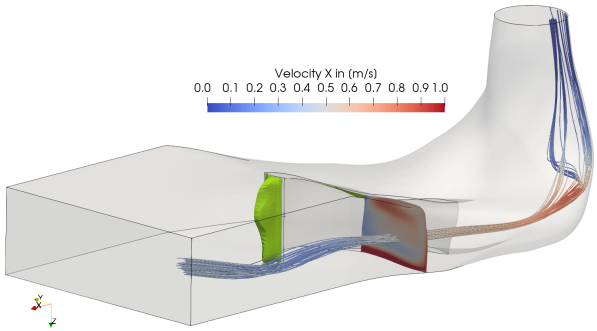

(d) Adjoint optimized design (IG: EA opt.).

Figure 13: Backflow and swirling behavior along the pier segment and in the outlet box.

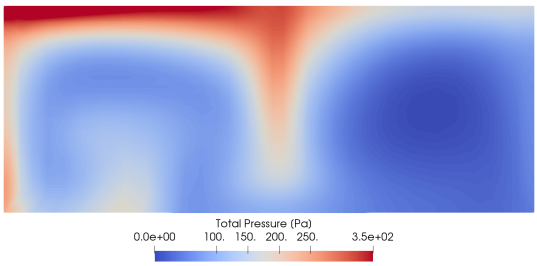

(a) Base design.

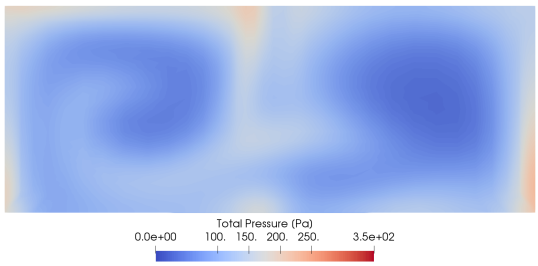

(b) Adjoint optimized design (IG: Base design).

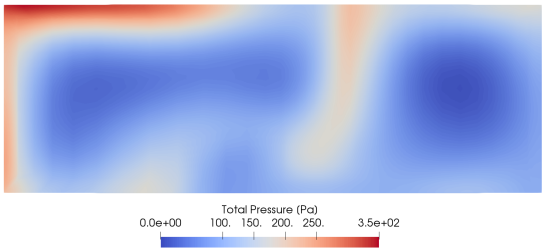

(c) EA optimized design.

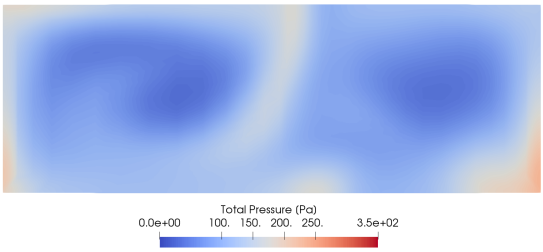

(d) Adjoint optimized design (IG: EA opt.).

Figure 14: Total pressure p_t at the outlet for full-load OP.

The not recovered kinetic energy at the draft tube outlet is present in form of swirl and flow non-uniformity, and is highlighted in the figures 14 (a-d) by showing the total pressure on the

outlet patch. The base design model (a) clearly shows the largest spread in total pressure peak to peak and distribution, followed by the EA optimized design (c) and the two adjoint solutions in the order (b) and (d), confirming the results in figure 12 (b).

6. Conclusions

In this work, a discrete adjoint solver implemented into the HSLU in-house coupled pressure-base CFD code was successfully applied to optimize the geometry of a draft tube base design as well as an EA optimized starting design.

The EA optimization used a set of 47 parameters to define the geometry during the optimization process. The main modification resulting from the EA optimization with regards to the base design was a shift in the position of the pier, therefore changing the area ratio of the two channels. The adjoint optimization on the other hand required no parametrization and instead used free-form deformation. This method allowed for more complex but still moderate geometries.

The advantages of the adjoint method is clear—compared to the EA optimization it was possible to reduce the computation time more then 30%, with a simultaneous additional improvement of the objective function by 14.48% starting from the base design. The combination of initial global EA optimization with subsequent adjoint optimization was able to minimize the total pressure losses along the draft tube most effectively (almost 22% compared to the base design). Investigation of the resulting flow fields revealed that the reduction in not recovered kinetic energy is the driving factor for the efficiency improvement, and is present in form of swirl and flow non-uniformity at the outlet. The results show that only the adjoint optimizations were able to reduce not only the overall losses, but also the local losses up to the end of the pier. All optimizations were able to eliminate the backflow region in the left channel of the pier segment. The findings of this paper suggest that the interplay between local and global optimization could be a promising strategy to find optimal geometries for multi-operating point/multi-objective optimization and will be further investigated, together with the consideration of additional operating points, in subsequent research.

Acknowledgements

The authors would like to thank Innosuisse, the Swiss innovation agency, for financial support.

References

Bibliography

[1] J. McNabb, C. Devals, S. A. Kyriacou, N. Murry, and B. F. Mullins, "CFD based draft tube hydraulic design optimization," *IOP Conf. Ser.: Earth Environ. Sci.*, vol. 22, 2014, 012023.

[2] S. Bahrami, C. Tribes, C. Devals, T. C. Vu, and F. Guibault, "Multi-fidelity shape optimization of hydraulic turbine runner blades using a multi-objective mesh adaptive direct search algorithm," *Applied mathematical modelling*, vol. 40, no. 2, pp. 1650–1668, 2016.

[3] A. Semenova, D. Chirkov, A. Lyutov, S. Chemy, V. Skorospelov, and I. Pylev, "Multi-objective shape optimization of runner blade for kaplan turbine," in *IOP Conference Series: Earth and Environmental Science*, IOP Publishing, vol. 22, 2014, p. 012 025.

[4] S. Kyriacou, E. Kontoleontos, S. Weissenberger, L. Mangani, E. Casartelli, I. Skouteropoulou, M. Gattringer, A. Gehrer, and M. Buchmayr, "Evolutionary algorithm based optimization of hydraulic machines utilizing a state-of-the-art block coupled cfd solver and parametric geometry and mesh generation tools," in *IOP Conference Series: Earth and Environmental Science*, IOP Publishing, vol. 22, 2014, p. 012 024.

[5] A. Alnaga and J.-L. Kueny, "Optimal design of hydraulic turbine distributor," *WSEAS Transactions on Fluid Mechanics*, vol. 2, no. 3, pp. 175–185, 2008.

[6] H. Kawajiri, Y. Enomoto, and S. Kurosawa, "Design optimization method for francis turbine," in *IOP Conference Series: Earth and Environmental Science*, IOP Publishing, vol. 22, 2014, p. 012 026.

[7] L. Mangani, M. Buchmayr, and M. Darwish, "Development of a novel fully coupled solver in openfoam: Steady-state incompressible turbulent flows," *Numerical Heat Transfer, Part B: Fundamentals*, vol. 66, no. 1, pp. 1–20, 2014.

[8] J. E. Peter and R. P. Dwight, "Numerical sensitivity analysis for aerodynamic optimization: A survey of approaches," *Computers & Fluids*, vol. 39, no. 3, pp. 373–391, 2010.

[9] A. Haroutunian, G. Francois, J.-Y. Trepanier, and T. Vu, "Draft tube pier leading edge shape optimization," in *24th Symposium on Hydraulic Machinery and Systems*, IAHR, 2008.